Allosteric inhibition of *Staphylococcus aureus* D-alanine:D-alanine ligase revealed by crystallographic studies

Shenping Liu[†], Jeanne S. Chang, John T. Herberg, Miao-Miao Horng, Paul K. Tomich[‡], Alice H. Lin[§], and Keith R. Marotti

Pfizer, Inc., Eastern Point Road, Groton, CT 06340

Edited by Brian W. Matthews, University of Oregon. Eugene, OR, and approved August 21, 2006 (received for review June 14, 2006)

D-alanine:D-alanine ligase (DDl) is an essential enzyme in bacterial cell wall biosynthesis and an important target for developing new antibiotics. It catalyzes the formation of D-alanine:D-alanine dipeptide, sequentially by using one D-alanine and one ATP as substrates for the first-half reaction, and a second D-alanine substrate to complete the reaction. Some gain of function DDl mutants can use an alternate second substrate, causing resistance to vancomycin, one of the last lines of defense against life-threatening Gram-positive infections. Here, we report the crystal structure of *Staphylococcus aureus* DDl (StaDDl) and its cocrystal structures with 3-chloro-2,2-dimethyl-*N*-[4(trifluoromethyl)phenyl]propanamide (inhibitor 1) (K_i = 4 μM against StaDDl) and with ADP, one of the reaction products, at resolutions of 2.0, 2.2, and 2.6 Å, respectively. The overall structure of StaDDl can be divided into three distinct domains. The inhibitor binds to a hydrophobic pocket at the interface of the first and the third domain. This inhibitor-binding pocket is adjacent to the first D-alanine substrate site but does not overlap with any substrate sites. An allosteric inhibition mechanism of StaDDl by this compound was proposed. The mechanism provides the basis for developing new antibiotics targeting D-alanine:D-alanine ligase. Because this compound only interacts with residues from the first D-alanine site, inhibitors with this binding mode potentially could overcome vancomycin resistance.

antibiotic | crystallography | inhibition mechanism | kinetics | cell wall synthesis

Many commonly prescribed antibiotics target bacterial cell wall biosynthesis. Penicillin, the first natural antibiotic discovered, and β-lactam antibiotics of the cephalosporin family inhibit the cross-linking of cell wall peptidoglycan precursors by acylating the active sites of bacterial bifunctional transglycosylase/transpeptidases (1). Antibiotics in the vancomycin family bind to D-alanine:D-alanine termini of peptidoglycans and block their cross-linking to adjacent strands by transpeptidases (2). This blocking leads to weakened cell walls and bacterial cell lysis. Resistance to both antibiotic families has arisen because of extensive antibiotic usage and bacterial evolution. The most common type of β-lactam resistance stems from elimination of these antibiotics by β-lactamases (1). Production of alternative termini for the peptidoglycan precursors greatly reduces the binding affinity of vancomycin, resulting in vancomycin resistance (3). In the face of these resistance mechanisms, D-alanine:D-alanine ligase (DDl), another enzyme in the cell wall biosynthesis pathway, has emerged as an attractive target to develop new antibiotics.

The reaction catalyzed by DDl produces the precursor of the cell wall peptidoglycan, D-alanine:D-alanine dipeptide (4), and consists of two half-reactions. In the first half-reaction, DDl uses ATP and D-alanine to produce a phosphorylated D-alanine intermediate. In the second half-reaction, WT DDl uses D-alanine as the second substrate, which leads to the normal D-alanine:D-alanine dipeptide product, whereas some gain-of-function DDl mutants preferentially use other D-amino acids as the second substrate. For example, in phenotypes of VanA and VanB (vancomycin-resistant *enterococci*) D-lactate is used as the second substrate. In VanC, D-serine is used (5). The switch from a D-alanine:D-alanine termini to D-alanine:D-X leads to a significant reduction in the binding affinity of vancomycin and vancomycin resistance (5). DDl is essential for bacteria development (K.R.M. and D. Romero, unpublished data) and has no human ortholog and, thus, is an ideal target for the treatment of infectious diseases.

Early kinetic studies on DDl revealed two distinct D-alanine-binding sites with very different affinities (6, 7) (see also Table 1). The high-affinity site is for the first (N-terminal) D-alanine of the reaction, whereas the second (C-terminal) D-alanine has much lower affinity (6, 7). As a structural analog of D-alanine, the antibiotic D-cycloserine was found to inhibit DDl competitively and reversibly (8–10). The tight binding of D-cycloserine to DDl suggests that the antibiotic binds to the high-affinity D-alanine site (10). Compounds designed to mimic the D-alanine:D-alanine dipeptide or the reaction transition-state intermediates led to the developments of phosphinate and phosphonate dipeptide analogs (11–12). These phosphinates or phosphonates, after being phosphorylated by DDl, bind to the protein tightly and inhibit the reaction (11–12). The best *in vitro* IC_{50} of these compounds are $\approx$4 μM on *Streptococcus faecalis* DDl, and their antibacterial activities are not significant (11). Generally they are much less active against vancomycin-resistant causing DDl from *Enterococcus faecium* BM4147 (VanADDl) (ref. 12; Table 1).

The atomic resolution structures of DDl are important in understanding its catalytic mechanism and developing new antibiotics targeting it to overcome vancomycin resistance. Four crystal structures of D-alanine:D-X ligases have been previously reported. These structures are the WT and Y216F mutant of type B DDl from *Escherichia coli* (EcoliDDlB) (13, 14), which causes no vancomycin resistance; the D-alanine:D-lactate ligase from *Leuconostoc mesenteroides* (LmDDl2) with mild vancomycin resistance (15); and VanADDl, which causes high level of vancomycin resistance (16). These crystals were obtained in the presence of phosphinate or phosphonate analogs. The structures

Author contributions: S.L. designed research; S.L., J.S.C., J.T.H., M.-M.H., P.K.T., and A.H.L. performed research; S.L., J.S.C., J.T.H., P.K.T., and K.R.M. contributed new reagents/analytic tools; S.L., M.-M.H., P.K.T., and K.R.M. analyzed data; and S.L. and K.R.M. wrote the paper.

The authors declare no conflict of interest.

This paper was submitted directly (Track II) to the PNAS office.

Abbreviations: DDl, D-alanine:D-alanine ligase; StaDDl, *Staphylococcus aureus* DDl; LmDDl2, *Leuconostoc mesenteroides* DDl; VanADDl, vancomycin-resistant causing DDl from *Enterococcus faecium* BM4147; inhibitor **1**, 3-chloro-2,2-dimethyl-*N*-[4(trifluoromethyl)phenyl]propanamide.

Data deposition: The atomic coordinates have been deposited in the Protein Data Bank, www.pdb.org (PDB ID codes 2I80, 2I87, and 2I8C).

[†]To whom correspondence should be addressed. E-mail: shenping.liu@pfizer.com.

[‡]Present address: 3703 Blackberry Lane, Kalamazoo, MI 49008.

[§]Present address: 3720 Pine Tree Terrace, Portage, MI 49024.

www.pnas.org/cgi/doi/10.1073/pnas.0604905103

Table 1. DDl ligand-binding affinities

Compound	Inhibitor **1**	ATP	First D-alanine	Second D-alanine	D-cycloserine	Phosphinate/phosphonate
Affinity, μM	4.0	60.0	25.0	1,500	3	2 and 750*

All data generated from this study on StaDDl, except phosphinate/phosphonate.
*Data of the best compound (D-Ala[$PO_2^-CH_2$]D-Phe) on free EcoliDDlB and VanADDl are from ref. 12.

revealed ADP and a phosphorylated phosphinate or phosphonate that mimics the tetrahedral transition state intermediate of the second half-reaction. Based on these structures the two D-alanine-binding sites were mapped and a common catalytic mechanism for DDl was proposed. The preference of VanADDl for D-lactate as the second ligand was proposed to be mediated by mutated residues at the second D-alanine site (16). As a proof of concept, gain of VanADDl activities could be obtained from active site mutants of type B DDl from *E. coli*, designed base on x-ray structures predictions (17).

Presently, D-cycloserine is the only antibiotic targeting DDl; however, toxicity limits its usage. For the initial development of safe and effective inhibitors of this enzyme, we chose DDl of *Staphylococcus aureus*, a Gram-positive pathogen mutant of which cause deadly outbreaks of community-associated meticillin-resistant infections (18), as the prototype. Several compounds exhibiting moderate potencies (4–50 μM) were identified in a high-throughput screen against *Staphylococcus aureus* D-alanine:D-alanine ligase (StaDDl). One of these inhibitors, 3-chloro-2,2-dimethyl-*N*-[4(trifluoromethyl)phenyl]propanamide (inhibitor **1**) (see Fig. 2*A*), is structurally distinct from either ADP or D-alanine and was selected for follow-up because a novel binding mode was anticipated. The apparent K_i (4 μM) of inhibitor **1** on StaDDl is clearly comparable with the best of the existing DDl inhibitors (Table 1). In this paper, we report a previously undescribed structure of StaDDl and reveal through crystallographic and kinetic analysis that inhibitor **1** inhibits StaDDl through an allosteric mechanism.

Results

Overall Structure. There are two StaDDl monomers forming a dimer in the crystallographic asymmetric unit. The StaDDl monomer can be divided into three α/β domains: domain 1, from N terminus to 120; domain 2, 121–218; and domain 3, 219 to the C terminus (Fig. 1). Except for some disordered loops mentioned below, the two StaDDl molecules in the asymmetric unit are well defined in all three crystal structures, with continuous electron density from residues 3 to 358 for monomer A and 3–360 for monomer B (two additional histidine residues contributed from the C-terminal His tag). In the apo, inhibitor, and ADP·Mg^{2+}-bound StaDDl structures described here, and previously published ligand-free LmDDl2 monomer structure (15), the peptide 244–258 regions are disordered with no visible electron density (Fig. 1). Interestingly, this peptide region, named ω-loop, plays an important role in substrate recognition and binding. In the previously reported DDl structures complexed with phosphorylated phosphonate or phosphinate and ADP·Mg^{2+}, this loop is ordered (13–16). In the apo StaDDl and ADP·Mg^{2+} cocrystal structures, peptides S14-E16 and H96-E101 exhibit very weak electron density. The equivalent regions in other DDls interact with the first D-alanine substrate (13–16). In inhibitor cocrystal structure, inhibitor **1** and peptides S14-E16 and H96-E101 have well defined electron densities in both monomers (Fig. 2*B*). In the ADP·Mg^{2+} structure, although ATP, magnesium, and D-alanine were used for cocrystallization, the electron density maps showed density only for an ADP molecule and one magnesium ion in each monomer (ligands are much more ordered in B molecule; Fig. 2*C*). Except for these differences, there are no significant global conformation changes between structures obtained from different crystals, or different monomers in the same crystal (the rmsd values range from 0.47 to 0.9 Å for all visible Cα atoms).

Ligand-Binding Sites. Inhibitor **1** was found to bind to a site formed by residues at the interface of the first and the third domain of the protein (Fig. 1 and 2*D*). Most of these residues are hydrophobic and well conserved across the DDl superfamily (Fig. 2*D*). The orientation of the inhibitor in the binding pocket is such that the trifluromethyl group locates at the bottom of the binding pocket and the chloropropanamide group points out to the entrance of the pocket. Side chains of F313 and M310 are located on opposite edges of the benzene rings of the inhibitor, and those of L94 and P311 sandwich each face. The side chains of F92, L289, V117, and L337 form the bottom wall of this pocket. At the entrance of the binding pocket, there are residues E16, V19, and H96, which are strictly conserved across the entire DDl family. The chlorine of the inhibitor sits on top of the face of the side chain of H96. In DDl structures with transition state analog bound, the first D-methyl group of the analog interacts similarly with the equivalent histidine side chain (13–16). The only hydrogen bond observed is that between the amide of the inhibitor and the carbonyl oxygen of P311 (Fig. 2*D*).

The ADP-binding site is located at a cleft between the second and the third protein domains. Interactions of ADP with DDl include hydrophobic, ion pairs, and hydrogen bonds (Fig. 2*E*). The N6 atom of the base donates hydrogen bonds to the side chain Oε atom of E213 and the main chain oxygen of Q214, respectively, and N1 and N7 receive hydrogen bonds from the main chain amine of V216 and the side chain of K177, respectively. This hydrogen bond pattern is apparently specific toward the adenine base. The base also makes π–π stacking interactions with the aromatic side chain of F175 and an edge-on interaction with that of F295. In addition, the side chains of V216 and L145

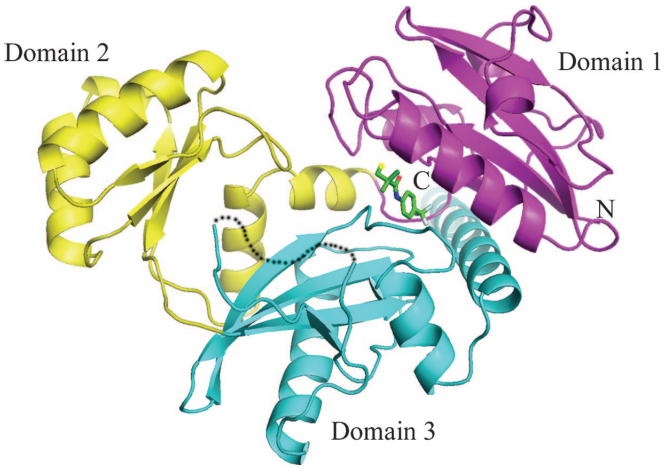

Fig. 1. Overall structure of StaDDl in ribbon diagram. Domains 1, 2, and 3 are colored in magenta, yellow, and cyan, respectively. Inhibitor **1** in stick model is included to show its location. In Figs. 1–4 and 6, carbon, oxygen, nitrogen, fluorine, chlorine, and phosphor atoms are colored green, red, cyan, blue, yellow, and brown, respectively, except noticed. The missing ω-loop is shown in dash. This picture was generated by using graphic program PyMol (19).

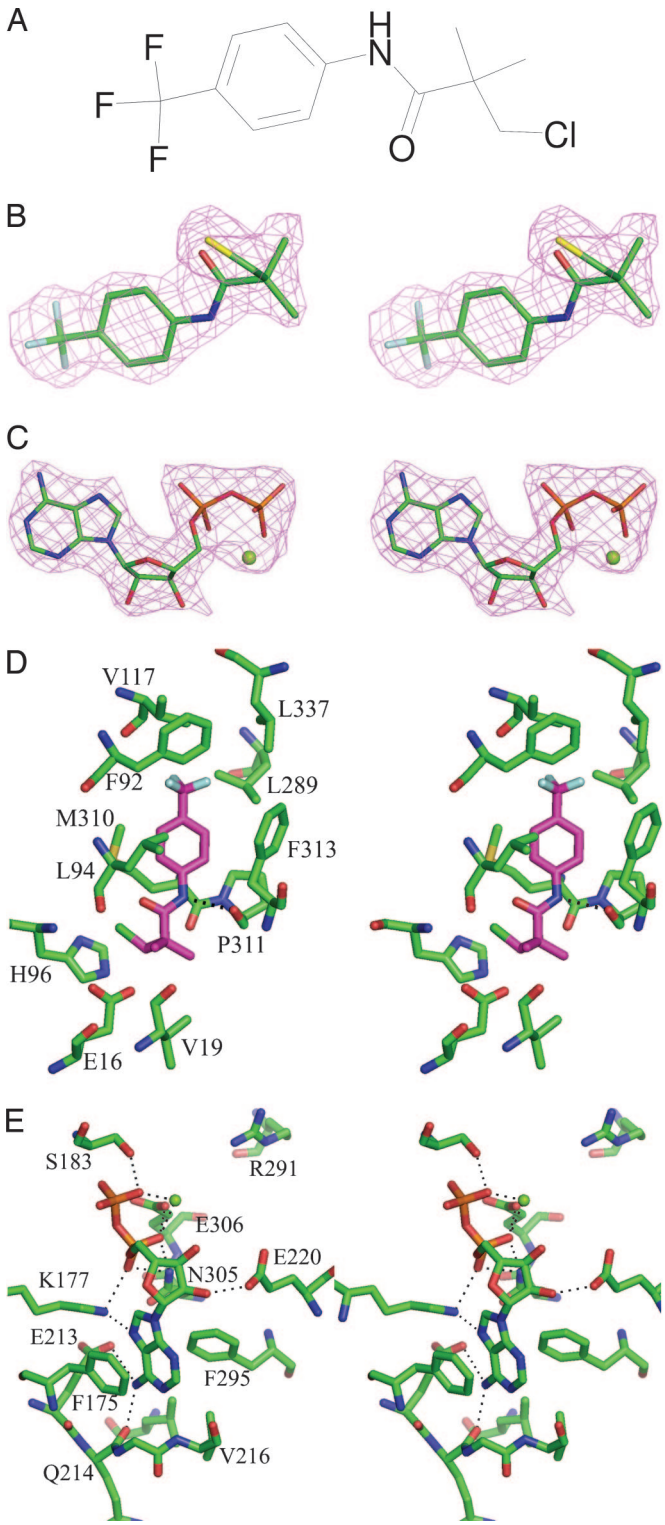

Fig. 2. Ligand-binding sites of StaDDl. (*A*) Chemical structure of inhibitor **1**, a small molecule inhibitor of StaDDl from high-throughput screen. (*B*) A stereoview of inhibitor **1** (sticks) embedded in $2F_o - F_c$ type electron density contoured at 1.2σ (pink). (*C*) A stereoview of ADP (sticks) and Mg^{2+} (green ball) embedded in $2F_o - F_c$ type electron density contoured at 1.0σ (pink). (*D*) A stereoview of the binding pocket of StaDDl for inhibitor **1**. Residues interacting with inhibitor are labeled. Hydrogen bond is shown in dash. Ligand carbon atoms are colored magenta for clarity. (*E*) A stereoview of binding interactions of ADP and Mg^{+2} ion with StaDDl. R291 side chain also is shown to indicate the D-alanine site. Same color scheme as *D*.

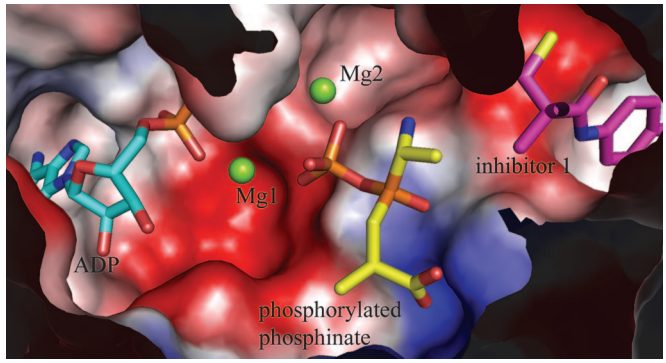

Fig. 3. A composite surface representation of StaDDl ligand-binding sites. The electrostatic protein surface was constructed from apo StaDDl structure, with red and blue representing negative and positive charges, respectively, white is for neutral. Ligands are in stick model. ADP and the first Mg^{2+} (Mg1) are from ADP+Mg^{2+}-bound StaDDl structure. The phosphorylated phosphinate and the second Mg^{2+} (Mg2) are modeled in from substrates bound LmDDl2 monomer by superimposition by using program LSQMAN (20). Inhibitor **1** is from inhibitor 1–StaDDl complex. For clarity, the carbon atoms of ADP, phosphinate, and inhibitor **1** are shown in cyan, yellow, and magenta color, respectively.

also make hydrophobic interactions with the base. The O2′ of the ribose ring establishes strong hydrogen bonds with the side chain of E220 (Fig. 2*E*), but O3′ lacks hydrogen partner. The α- and β-phosphates of ADP form ion-pair interactions/hydrogen bonds with the side chains of K177 and N305 and are bridged by a Mg^{2+} ion, held in position by coordination interaction with the side chain of E306. The β-phosphate also forms hydrogen bonds with S183 Oγ atom. S183 is located at a Gly-rich loop that interacts with ADP phosphate in other DDl structures (13–16). The only significant changes upon ADP binding are the side chains of F175 and F295, which move closer to the adenine base to form protein–ADP interactions. The ADP-binding site and the bound ADP conformation in our structure are very similar to those in previously reported DDl structures (13–16), except they lack any interactions with the disordered ω-loop.

The structures of DDl with bound phosphorylated phosphinate or phosphonate inhibitors from other species show that these transition state analogs are located at the intersection of the three domains (13–16). Although we did not obtain a substrate or substrate analog-bound StaDDl crystal structure, homology modeling enabled us to map two D-alanine-binding sites in the StaDDl structure (Fig. 3). Overall these D-alanine sites are positively charged and at the center are the side chain of the strictly conserved residue R291, the side-chain nitrogen of N308 and the main-chain amide of G312. These residues form an oxyanion hole that interacts with the terminal phosphate of the analog and, presumably, in a similar manner with the phosphate of the tetrahedral transition-state intermediate (Fig. 3). A sulfate ion was found at this position in our structures.

Inhibition Mechanism. The fact that there is no overlap between the inhibitor site, ATP/ADP site, or the mapped D-alanine sites (Fig. 3) excludes a competitive inhibition mechanism with either ATP or D-alanine. The closest distance between the inhibitor and any of the substrates is 3.6 Å and is between the 2-methyl group of the inhibitor and the modeled methyl group of the first D-alanine substrate. Kinetic studies on StaDDl were carried out to characterize StaDDl and to establish the inhibition mechanism of our inhibitor. The initial velocities versus concentration curves follow Michaelis–Menten kinetics. The measured binding affinity of StaDDl for ATP, $K_{m,app,ATP}$, is 60 μM, and the specific activity for the StaDDl was determined to be 0.08

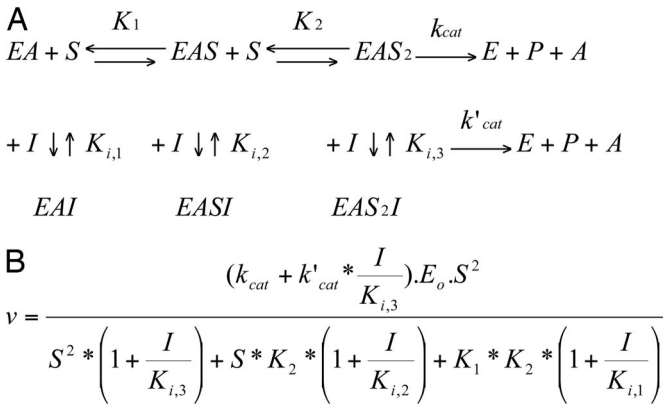

Fig. 4. Kinetic analysis of inhibitor **1**. (*A*) Catalytic reaction and inhibition of DDl. *E*, *EA*, *EAS*, and *EAS2* stand for the free enzyme, the enzyme–ATP complex, and the enzyme–ATP complex with 1 or 2 D-alanine substrates bound, respectively; *EAI*, *EASI*, and *EAS2I* stand for inhibitor complex with these species. (*B*) Multiple curve data fitting for inhibition velocity. Fitting statistic values are listed (Fig. 6, which is published as supporting information on the PNAS web site). *E0*, *I*, and *S*, are the total enzyme, inhibitor, and D-alanine concentration respectively. k_{cat} E_0 and k'_{cat} E_0 are V_{max} and V'_{max}, the maximum velocity for uninhibited and *EAS2I* complex, respectively, and K_1, K_2, the Michaelis–Menten constant values for the first and second D-alanine-binding sites. K_{i1}, K_{i2}, and K_{i3}, are the inhibition constants toward *EA*, *EAS*, and *EAS2* complex, respectively.

μmol·min^{-1}·mg^{-1}. Two D-alanine sites with distinguishable affinities ($K_{m,1}$ = 0.025 mM and $K_{m,2}$ = 1.5 mM) were identified (Table 1). These values are similar to those reported for *ddlA*, *ddlB* of *E. coli* ligase and *Salmonella typhimurium* ligase (10, 21).

To simplify the interpretation of the inhibition mechanism, ATP (1 mM) was present in excess and premixed with the enzyme (1 mM, $\gg$60 μM). Under these conditions, SdaDDl exists only as an enzyme–ATP complex, and only inhibitions against D-alanine need to be considered. Affinities of our inhibitor to different protein species were measured by using multiple curves data-fitting algorithm to reaction velocity with varying D-alanine and inhibitor concentrations (Fig. 4). The fitted kinetic data showed the inhibitor is able to bind to the protein species with zero, one, or two D-alanine sites occupied ($K_{i,1}$, $K_{i,2}$ $K_{i,3}$ = 19.5 ± 9.5, 33.4 ± 2.6, and 144 ± 12; Fig. 4), and the inhibitor-bound complex is nonproductive (k'_{cat} = 0; Fig. 4). This analysis characterizes the mode of inhibition by inhibitor as noncompetitive.

Given that inhibitor **1** does not cause global conformational changes in StaDDl (see *Discussion*), the most plausible manner to inhibit the enzyme is to locally disturb the formation of a productive active site. The common catalytic mechanism proposed for the reaction based on known DDl structures is that the D-methyl group of the first D-alanine interacts with a conserved His and Val residues (H96 and V19), and the amine of D-alanine interacts with a conserved Glu (E16) (Fig. 5). These interactions serve to orient either the first D-alanine to accept the γ-phosphate from ATP or the phosphorylated form for reaction with the incoming second D-alanine. Thus, the binding of our inhibitor to DDl prevents these residues from moving into active positions and interferes with the orientation of the first D-alanine substrate (Fig. 5).

Discussion

We did a conformational analysis to see whether inhibitor **1** binding causes large conformational changes. We chose the structure of LmDDl2 to analyze the conformational changes upon substrate binding. In the LmDDl2 dimer, one monomer is ligand-bound, whereas the other is ligand-free (15). This structure allowed us to distinguish the conformation changes due to ligand binding from those due to sequence differences. The conformations of the StaDDl monomers and the ligand-free LmDDl2 monomer are very similar, with most secondary structures superimposable (rmsd 0.9 Å for 232 Cα from all three domains; Fig. 7*A*, which is published as supporting information on the PNAS web site). The largest structural difference occurs around the peptide sequence N54 to S85 of StaDDl. This peptide has the highest sequence variation between different DDl sequences. In StaDDl, these residues form a long β-strand followed by a short α-helix. In LmDDl2, they form two α-helices and are located at quite different positions. Another peptide with the largest sequence variation occurs around the ω-loop, which is absent in both structures.

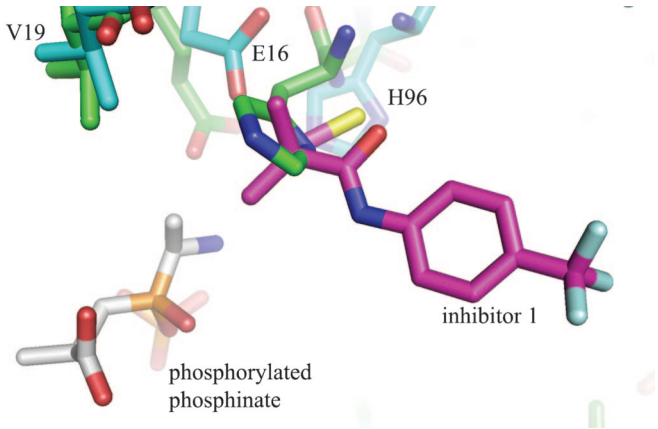

Fig. 5. Structure superposition of inhibitor **1**-bound StaDDl with reaction intermediate analog bound LmDDl2. Residues essential for the first half-reaction are labeled (see text). For clarity, carbon atoms of StaDDl, inhibitor **1**, and phosphinate are colored cyan, magenta, and white, respectively.

There are significant conformational changes between our StaDDl structures and that of the ligand-bound monomer of LmDDl2 (Fig. 7*B*). The individual domains can be superimposed better (0.78–1.0 Å) than the molecule as a whole. To summarize these changes, one can imagine DDl as an upturned right hand: the thumb is the first domain, the fingers are formed by the second domain and the third domain composes the palm. Upon binding substrates, the second domain moves closer to the third domain to interact with both substrates. This movement also brings about a change in the position of the ω-loop such that it now covers the substrate-binding cleft and is stabilized by interactions with both substrates. Along with the second domain, ADP also shifts ≈1.1 Å toward the two D-alanine sites. The first domain does not make significant global movements, but some local conformation changes are observed (Fig. 7*B*). Clearly, substrate-bound LmDDl2 is in a "closed" form and StaDDl in our crystals is in an "open" form. Interestingly, the ADP·Mg^{2+}-bound StaDDl is also in the open form, presumably because the binding of reaction products does not provide the necessary interactions to convert the protein to the closed form, suggesting a role of a "molecular glue" for the γ-phosphate of ATP.

Our kinetic studies provide compelling evidence that the inhibitor used in our study is a pure noncompetitive inhibitor because it does not interfere with the binding of D-alanine to either site or that of ATP, but instead leads to the formation of an unproductive enzyme–substrate–inhibitor complex. Structural analysis provides an interpretation of this type of inhibition at the atomic level. The binding of our inhibitor to StdDDl does not inhibit the conformation changes in the second domain upon binding ATP nor the binding of D-alanine to either the first or second site, but rather works in a manner to change the

orientation of the first D-alanine via interactions through the D-methyl and amino groups that results in a misalignment of this substrate preventing it from completing the first half-reaction.

This mode of inhibition is of great interest because it is significantly different from that of existing DDl inhibitors such as phosphinate, phosphonate, and D-cycloserine. Inhibitors of this nature provide the opportunity to develop compounds that have superior cellular absorption and metabolic properties and safety profiles. The small size of inhibitor **1** provides sufficient scope for elaboration of the molecule. Further, because the compound only interacts with key residues near or at the first D-alanine site, inhibitors developed from it or inhibitors that exploit these interactions have the potential to overcome vancomycin resistance.

We also conducted a sequence alignment to assess how specific this binding pocket is (Fig. 8, which is published as supporting information on the PNAS web site). Residues F92-L95 are quite conserved across the chosen DDl sequences. Among these sequences, the equivalents of V118, M310, P311, F313, and L337 in other DDls also may interact favorably with the inhibitor. The only residue that may interfere with inhibitor binding is the one that is equivalent to L289 in DDls from some Gram-negative pathogens: At this position, the side chain of E299 in the LmDDl2 structure extends into this binding pocket. On the other hand, the sequence of DDl from the Gram-positive vancomycin-resistant strain (VanA) seems to be compatible with inhibitor binding (Fig. 8).

In conclusion, the chemical template represented by the inhibitor presented here may bind and inhibit DDl from other pathogens, especially those of Gram-positive organisms. Residues interacting with ATP/ADP and the first D-alanine substrate are highly conserved. On the other hand, there are some variations on the residues interacting with the second D-alanine substrate (Fig. 8). This fact may explain why different DDls have different specificity toward the second substrate.

Materials and Methods

Protein Expression and Purification. StaDDl was identified in the Human Genome Sciences *S. aureus* database by using a homology search with *E. coli* DDl. The *S. aureus* gene was isolated by polymerase chain amplification by using primers containing a NcoI site at the 5′ end and a HindIII site at the 3′ end of the gene. The gene was cloned into the expression vector pQE-60 that encodes a 6x His tag at the carboxyl terminus of the protein. The StaDDl gene then was expressed in *E. coli* M15 (pREP4). Expressed protein was purified by using an affinity column of 50 ml NTA immobilized nickel resin (Qiagen, Valencia, CA). Purified protein was stored at −80°C in buffer containing 50 mM Tris·HCl (pH 8.0) and 1 mM DTT.

Crystallization and Data Collection. The enzyme was crystallized by the hanging-drop-vapor diffusion method against a well solution of 30–35% PEG monomethyl ether 500/100 mM Mes (pH 6.0)/100 mM Li_2SO_4. Drops were formed by adding 2 μl of well solution into 2 μl of protein solution (10 mg/ml/50 mM Tris·HCl (pH 8.0)/1 mM DTT). For cocrystallization with inhibitor, a stock solution of 30 mM compound was dissolved in dimethyl sulfoxide and mixed with a protein solution (10 mg/ml) to a final concentration of 1 mM. For cocrystallization with substrates, stock solutions of 100 mM were added to a final concentration of 1 mM ATP–magnesium and 1 mM D-alanine, respectively. Crystals usually appear overnight and reach 0.3·0.2·0.2 mm in several days. Crystals were briefly soaked in mother liquor with 45% PEG monomethyl ether and then flash frozen in liquid nitrogen. Crystal data were collected at APS IMCA beam-line 17-ID at 100 K. All three crystals have the same crystal form of the space group $P2_1$, with typical unit cell constants of a = 68.09, b = 66.27 and c = 79.11 Å, and β = 96.23°. The data were reduced by using program suite HKL2000 (22) and converted with CCP4 program suite (23) to formats suitable for other programs (Table 2).

Table 2. X-ray data collection and structure refinement statistics

Crystal	apo	Inhibitor **1**	ADP + Mg^{2+}
Data collection			
Independent reflections	46,823	33,377	25,017
Resolution, Å	2.0	2.2	2.5
Completeness, %	99.7 (100)	94.1 (76.3)	99.0 (99.2)
R_{merge}, %	3.8 (16.2)	5.2 (17.7)	7.0 (62.1)
I/σ	26.9 (4.5)	21.5 (3.81)	23.9 (2.0)
Refinement			
Reflections used	44,471	31,696	23,741
R_{free} set	2,336	1,667	1,254
R factor, %	20.3 (18.7)	18.9 (18.6)	20.8 (28.1)
R_{free}, %	24.6 (26.1)	25.1 (28.7)	25.6 (31.7)
rms bonds, Å	0.023	0.019	0.020
rms angles, °	1.93	1.72	1.86
No. of water molecules	91	80	0
Avg B factor (protein, water, and ligand)	38, 35, —	33, 29, 29	55, —, 63

Numbers in parentheses are those in the highest resolution shell (2.0–2.05, 2.19–2.25, 2.50–2.59 Å, respectively). $R_{merge} = \Sigma|I - \langle I\rangle|/\Sigma\langle I\rangle$, where I is the integrated intensity of a given reflection. The average B factor for ligand in ADP + Mg crystal is for B molecule only.

Structure Determination and Refinement. Both crystal packing and self-rotation calculations suggested a dimer in the crystallographic asymmetric unit. The apo StaDDl structure was determined by a molecular replacement method with program MOLREP (24), with a LmDDl2 dimer as a search model (PDB code 1EHI; ref. 8). Refinements were carried out by using the program CNX (25) or REFMAC5 (26), and all model rebuilding was accomplished by using program O (27). Before refinement, 5% of the reflection data common to all crystal data sets were set aside for cross-validation analysis (28). The initial apo structure model that resulted from the molecular replacement search was subject to several rounds of rigid body refinements followed by replacement of the residues corresponding to StaDDl sequence and fitting to the electron density. Insertions and deletions between StaDDl and the search model initially were omitted and were rebuilt at a later stage. Because electron density showed some local variations between the two monomers in the dimer, noncrystallographic symmetry restraints were not used in the refinements. After extensive refinement, solvent molecules were located in difference electron density map at peaks $>3.5\sigma$. Initial complex structures were obtained from the refined apo structure, striped of all solvent molecules, followed by several cycles of rigid body refinement. Ligands were recognized and built in $2F_o - F_c$ and $F_o - F_c$ types of the electron density map, contoured at 1.0σ and 3.0σ, respectively. All structures were refined to low R factors and R_{free}, with 99.5% residues in allowed Ramachandran zones (Table 2).

Protein Inhibition Assay. To assay the activity of the enzyme, the reaction catalyzed by DDl was coupled with 2-amino-6-mercapto-7-methylthioguanosine (Berry and Associates, Inc., Ann Arbor, MI) and bacterial purine nucleoside phosphorylase (Sigma, St. Louis, MO) system for continuous detection of the inorganic phosphate product (29). The assay buffer mixture contained a final concentration of 50 mM Tris·HCl, pH 7.5/100 mM KCl/4 mM $MnCl_2$/200 μM 2-amino-6-mercapto-7-methylthioguanosine/1 unit/ml purine nucleoside phosphorylase. Addition of the substrate ATP or D-alanine premixed with enzyme was as specified. The assays were conducted in a 384-well μ-titer plate format. Reagent mixtures were added in a defined

order. The time course kinetic data were collected by recording the absorbance at 360 nm at room temperature for 20 min on the Spectramax-Plus 384 plate reader (Molecular Devices, Sunnyvale, CA). The absorbance measurements were converted to concentrations of the released inorganic phosphate product, and the linear portion of the product versus time curve was used to calculate the initial rate for each well. Data analysis software Origin 6.1 (OriginLab Corp., Northampton, MA) was used for kinetic mechanism data analyses by using a nonlinear least square-fitting algorithm.

We thank the former Pharmacia Bacterial Genomic Team at Kalamazoo (colead by Keith Marotti and Donna Romero) and specifically Yoshi Yagi and Steve Conrad for the HTS of DDl and team chemists for the hit triaging that led to the identification of inhibitor **1** and its selection for kinetic evaluation; the Pfizer antibacterial team at Groton for helpful discussions; Tim Benson, Eric T. Baldwin, William Watt, and Barry Finzel and other members of x-ray group of legacy Pharmacia at Kalamazoo for help on data collection and structure determination; and Seungil Han, Felix Vajdos, Jay Pandit, Xiayang Qiu, and, particularly, Andrew P. Seddon for their comments on the manuscript.

1. Spratt BG (1994) *Science* 264:388–393.
2. Groves P, Searle MS, Mackay JP, Williams DH (1994) *Structure (London)* 2:747–754.
3. Davies J (1994) *Science* 264:375–382.
4. Walsh CT (1989) *J Biol Chem* 264:2393–2396.
5. Arthur M, Reynolds P, Courvalin P (1996) *Trends Microbiol* 4:401–407.
6. Neuhaus FC (1962) *J Biol Chem* 237:778–786.
7. Neuhaus FC (1962) *J Biol Chem* 237:3128–3135.
8. Neuhaus FC, Lynch JL (1964) *Biochemistry* 3:471–480.
9. Strominger JL, Ito E, Threnn RH (1960) *J Am Chem Soc* 82:998–999.
10. Zawadzke LE, Bugg TDH, Walsh CT (1991) *Biochemistry* 30:1673–1682.
11. Parsons WH, Patchett AA, Bull HG, Schoen WR, Taub D, Davidson J, Combs PL, Springer JP, Gadebusch H, Weissberger B, *et al.*(1988) *J Med Chem* 31:1772–1778.
12. Ellsworth BA, Tom NJ, Bartlett PA (1996) *Chem Biol* 3:37–44.
13. Fan C, Moews PC, Walsh CT, Knox JR (1994) *Science* 266:439–443.
14. Fan C Park I, Walsh CT, Knox JR (1997) *Biochemistry* 36:2531–2538.
15. Kuzin AP, Sun T, Jorczak-Baillass J, Healy VL, Walsh CT, Knox JR (2000) *Structure (London)* 8:463–470.
16. Roper DI, Huyton T, Vagin A, Dodson G (2000) *Proc Nat Acad Sci* 97:8921–8925.
17. Park I, Lin C, Walsh CT (1996) *Biochemistry* 35:10464–10471.
18. Furuya EY, Lowy FD (2006) *Nat Rev Microbiol* 4:36–45.
19. DeLano WL (2002) The PyMOL Molecular Graphics System (DeLano Scientific, San Carlos, CA).
20. Kelywegt GJ, Jones TA (1994) *CCP4/ESF-EACBM Newsletter on Protein Crystallography* 31:9–14.
21. Daub E, Zawadzke LE, Botstein D, Walsh CT (1988) *Biochemistry* 27:3701–3708.
22. Otwinowski Z, Minor W (1997) in *Macromolecular Crystallography*, eds Carter JCW, Sweet RM (Academic, New York), Part A, pp 307–326.
23. Collaborative Computing Project #4, (1994) *Acta Crystallogr D* 50:760–763.
24. Vagin A, Teplyakov A (1997) *J Appl Cryst* 30:1022–1025.
25. Brünger AT (1992) XPLOR (Yale Univ Press, New Haven, CT), Version 3.1.
26. Murshudov GN, Vagin AA, Dodson EJ (1997) *Acta Crystallogr D* 53:240–255.
27. Jones TA, Zou J-Y, Cowan SW, Kjeldgaard M (1991) *Acta Crystallogr A* 47:110–119.
28. Brünger AT (1992) *Nature* 355:472–474.
29. Webb MR (1992) *Proc Natl Acad Sci USA* 89:4884–4887.